Article

Not peer-reviewed version

Dynamics of Neutron Transfer in the Reaction $^{3}He+^{9}Be$

Aidos K. Azhibekov , Englik K. Almanbetova , Mikhail A. Naumenko , Kairat O. Mendibayev * , Sergey M. Lukyanov , Talgat G. Issatayev , Bakhytzhan A. Urazbekov , Asset M. Kabyshev * , Kuralay Dyussebayeva , Timur K. Zholdybayev

Posted Date: 30 October 2024

doi: 10.20944/preprints202410.2284.v1

Keywords: neutron transfer; DWBA method; FRESCO code; TDSE approach

Article

Dynamics of Neutron Transfer in the Reaction ^{3}He+^{9}Be

Aidos K. Azhibekov [1,2], Englik K. Almanbetova [1], Mikhail A. Naumenko [1], Kairat O. Mendibayev [1,3,*], Sergey M. Lukyanov [1], Talgat G. Issatayev [1,4], Bakhytzhan A. Urazbekov [4], Asset M. Kabyshev [4,*], Kuralay Dyussebayeva [5] and Timur K. Zholdybayev [3]

1 Joint Institute for Nuclear Research, Dubna, Russia
2 Korkyt Ata Kyzylorda University, Kyzylorda, Kazakhstan
3 Institute of Nuclear Physics, Almaty, Kazakhstan
4 L.N. Gumilyov Eurasian National University, Astana, Kazakhstan
5 Al-Farabi Kazakh National University, Almaty, Kazakhstan
* Correspondence: kayrat1988@bk.ru (K.O.M.); assetenu@gmail.com (A.M.K.)

Abstract: The paper presents the results of experiments on measuring cross sections for the neutron transfer channels ^{9}Be(^{3}He,α)^{8}Be$_{gs,3.03}$ in the reaction of the ^{3}He (30 MeV) ions with the ^{9}Be target. To describe the angular distributions, we use the Distorted Wave Born Approximation (DWBA) method (FRESCO code). The results of the theoretical analysis are in agreement with the experimental data. In addition, we perform calculations based on the solution of the time-dependent Schrödinger equation (TDSE) for the weakly bound neutron of the ^{9}Be nucleus. The TDSE approach allows us to determine the dynamics of the neutron transfer process and calculate the probabilities for the transfer and removal of the neutron of the ^{9}Be nucleus in the ^{3}He+^{9}Be reaction.

Keywords: neutron transfer; DWBA method; FRESCO code; TDSE approach

1. Introduction

Among stable weakly bound nuclei, the ^{9}Be nucleus is of great interest. It has a Borromean structure in the ground state [1–5] and is typically represented as a system of two α-clusters and a neutron [6–8]. For instance, the (α+n+α) structure of the ^{9}Be nucleus was considered in [9,10] using Feynman path integrals. Experimental works [7,11,12] on the cluster channels of the decay of the nucleus ^{9}Be are also in favor of the (α+n+α) structure. However, with some probability, the nucleus ^{9}Be can be in a state corresponding to a two-particle structure, as evidenced by the results of experimental works [13,14], where it was shown that the nucleus ^{9}Be can decay through the two-particle channels ^{9}Be→n+^{8}Be or ^{9}Be→α+^{5}He. Because the ^{9}Be nucleus is stable, it is much easier to be investigated compared to other Borromean nuclei.

Structural features of light nuclei are manifested in nucleon transfer reactions [15–19], for example, in the angular distributions of reaction products. The structure of the light nuclei d, ^{3}He, and α is well known, and thus they are often employed to induce direct reactions, either as beams or as targets [15–19].

The process of the neutron transfer in a reaction with the ^{9}Be nucleus is interesting due to the fact that the low binding energies of the neutron (1.666 MeV) and α-particle (2.462 MeV) should influence the dynamics and mechanism of the transfer. The interaction of deuterons and alpha particles with ^{9}Be at an energy of 10-30 MeV/nucleon has been studied taking into account its cluster structure in [20,21]. The interaction potential for the colliding nuclei was constructed within the framework of the double folding model using a three-body wave function. Calculations with the double folding potential carried out within the optical model (OM) and Distorted Wave Born

Preprints.org (www.preprints.org) | NOT PEER-REVIEWED | Posted: 30 October 2024 doi:10.20944/preprints202410.2284.v1

Approximation (DWBA) method provided good agreement between the theoretical cross sections and the experimental data.

In our previous works [16–21], we performed experimental and theoretical studies of the angular distributions of the products of nucleon and cluster transfer in the reactions $d+^{9}Be$ [17,20,21], $^{3}He+^{9}Be$ [16,18], and $^{6}Li+^{9}Be$ [19]. The obtained data were analyzed using the OM, the coupled reaction channel (CRC) method, and the DWBA method. The analysis of the experimental data showed the sensitivity of the cross sections to the potential parameters in the exit channels. In works of other authors [22–24], experimental data on the neutron transfer in the $^{9}Be(^{3}He, \alpha)^{8}Be$ reaction channel were also analyzed within the DWBA method.

This paper presents a study of the neutron transfer process in the $^{9}Be(^{3}He,\alpha)^{8}Be$ reaction channel. To describe the mechanism and dynamics this process, the data are analyzed using the DWBA method [25–27] and the time-dependent Schrödinger equation (TDSE) approach [28–31]. A direct comparison of the theoretical description of the neutron transfer process (in our case, in the $d+^{9}Be$ reaction) within the framework of the stationary (DWBA) and time-dependent approaches (TDSE) is the challenge that we intend to tackle in this work. Each approach has its own advantages and disadvantages, but if used together, they complement each other. For this purpose, in the TDSE calculations, we used the values of the potential parameters obtained in the DWBA calculations for the $^{3}He+^{9}Be$ entrance channel and for the initial neutron wave functions. The TDSE approach allows for both qualitative (reaction dynamics) and quantitative analysis of the neutron transfer process (probabilities of neutron transfer and neutron removal, reaction channel cross sections) [32–34].

The study of the dynamics and mechanisms of nuclear reactions with the ^{9}Be nucleus is also important for applied research. For example, ^{9}Be can be used as a structural material for the thermonuclear reactors [35,36], and the mechanisms of the $^{3}He+^{9}Be$ reaction must be taken into account when designing a reactor structure and modeling the processes of burning of a dense hot plasma with the $d+^{3}He$ combination of nuclei in a metal ^{9}Be cylindrical liner [36]. ^{9}Be can also be used as a target for neutron sources due to the large cross section of the $^{9}Be(p,n)$ reaction [37,38].

2. Experiment

The experiment was performed on the U-120M cyclotron of the Nuclear Physics Institute, Řež, Czech Republic [39]. The ions of the ^{3}He beam (30 MeV) were incident on a self-supporting ^{9}Be foil target (2 mg/cm^2, 99%). Carbon and oxygen contaminations of the target were not observed in energy spectra. The average beam current was 10-20 nA [18,40].

To identify reaction products, energy loss ΔE and residual energy E_r were measured by four telescopes (ΔE-E method). Each telescope consisted of three silicon-lithium detectors with thicknesses of 10 μm (ΔE_1), 100 μm (ΔE_2), and 3 mm (E_r) and was protected by a 5 mm thick Cu–Pb collimator and a circular hole of 3 mm diameter [18,40]. The energy resolution of the detectors was ~ 150–200 keV (FWHM). The telescopes were located at a distance of ~ 25 cm from the target and could be rotated around it in the angular range of θ_{lab} = 7–63° with a step of 1–2°.

A typical example of a two-dimensional identification matrix obtained at an angle of θ_{lab} = 16° is shown in Figure 1a. It can be seen that A and Z of detected particles were unambiguously identified. The corresponding excitation energy spectrum of the ^{8}Be nucleus, which is a complementary product to the detected ^{4}He nucleus, is shown in Figure 1b. The first peak corresponds to the 0^+ ground state of ^{8}Be; the second peak is the 2^+ excited state. Thus, these two peaks confirm the corresponding reaction channels with the neutron transfer from ^{9}Be to ^{3}He. Thus, the used technique allowed us to measure the energy of the products, identify reaction channels, and obtain their corresponding differential angular distributions.

The outlined region in the ΔE_2-E_r plot [Figure 1a] was used to obtain the excitation energy plot [Figure 1b]. It can be seen that the 0+ ground state of ^{8}Be and the 2+ excited state are clearly separated. However, other reaction channels may contribute to the excitation energy plot in Figure 1b, in particular, breakup of ^{8}Be, because it can undergo breakup with alpha particle emission. In the peak of the 0+ ground state, the contribution of the background is insignificant. In the peak of the 2+ excited state, the contribution of the background, mainly associated with the breakup process $^{8}Be\rightarrow^{4}He+^{4}He$

with the threshold energy of –0.0918 MeV, is less than 15%; the contribution from the breakup of ^{9}Be is not present. To obtain the angular distributions presented in the next section, the background contribution was subtracted.

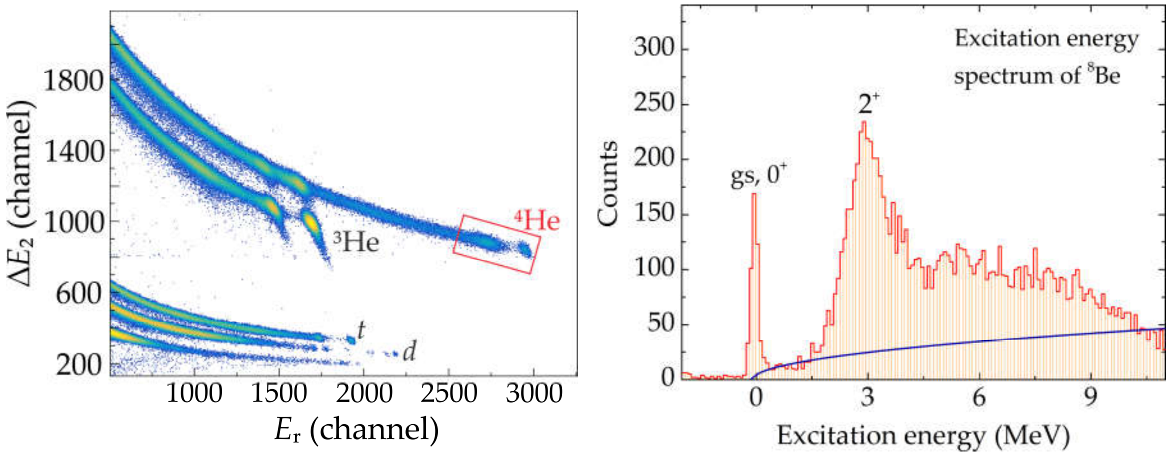

(**a**) (**b**)

Figure 1. (**a**) A typical example of a two-dimensional identification matrix obtained in the reaction ^{3}He+^{9}Be at E_{lab} = 30 MeV and θ_{lab} = 16°. (**b**) The corresponding excitation energy spectrum of the ^{8}Be nucleus; blue curve shows the background.

The following section presents the theoretical analysis of the experimental data on the reaction channels ^{9}Be(^{3}He,α)^{8}Be$_{gs,3.03}$. Detailed information on other channels of the ^{3}He+^{9}Be reaction can be found in our previous papers [18,40].

3. DWBA Calculations

Experimental differential cross sections for neutron transfer in ^{9}Be(^{3}He,α)^{8}Be$_{gs,3.03}$ reaction channels are shown in Figure 2. To describe the experimental data, we used the prior formalism of the DWBA amplitude [25,26] and the FRESCO code [27]. For calculating the cross sections of neutron (n) transfer reaction $A+b\rightarrow a+B$ ($A=a+n$, $B=b+n$), the formalism of the DWBA method requires the potentials of the entrance and exit channels, the spectroscopic amplitudes S_x for the neutron in the systems $A=a+n$ and $B=b+n$, and the potentials for calculating the neutron wave functions within the shell model.

The values of the spectroscopic amplitudes S_x = 0.791 for ^{9}Be=^{8}Be+n and S_x = –0.741 for ^{4}He=^{3}He+n were taken from our previous work [18]. The neutron wave functions were calculated within the shell model using the potential in the Woods-Saxon form with geometric parameters R = 1.25$A^{1/3}$ fm (radius) and a = 0.65 fm (diffuseness); the potential depths were adjusted to reproduce binding energies of a neutron.

As a starting point for searching for the optical potential U for the entrance and exit channels, we took the parameter sets from [18] (Table 1). These potential parameters have been successfully used to describe a large number of experimental data on the nucleon and cluster transfer channels in the ^{3}He+^{9}Be reaction. The potential U is defined as

$$U(r)=V_C(r)-V_V f(r;R_V,a_V)-iV_W f(r;R_W,a_W), \quad (1)$$

$$f(r;R_{V,W},a_{V,W})=\left[1+\exp\left(\frac{r-R_{V,W}}{a_{V,W}}\right)\right]^{-1}, \quad (2)$$

Preprints.org (www.preprints.org) | NOT PEER-REVIEWED | Posted: 30 October 2024 doi:10.20944/preprints202410.2284.v1

$$R_{V,W} = r_{V,W}\left(A_p^{1/3} + A_t^{1/3}\right), \quad (3)$$

$$V_C(r) = \begin{cases} \dfrac{Z_p Z_t e^2}{2R_C}\left[3 - \left(\dfrac{r}{R_C}\right)^2\right], r < R_C \\ \dfrac{Z_p Z_t e^2}{r}, r \geq R_C \end{cases}, \quad (4)$$

$$R_C = r_C\left(A_p^{1/3} + A_t^{1/3}\right), \quad (5)$$

where $V_C(r)$ is the Coulomb potential, Z_P and Z_t are the charges of the projectile and target, respectively; $V_{V,W}$ are the depths of the real and imaginary parts of the potential, respectively; $R_{V,W}$, $r_{V,W}$, and $a_{V,W}$ are their corresponding geometric parameters; A_P and A_t are the mass numbers of the projectile and target nuclei, respectively.

Table 1. Parameters of the optical potential (1) used in DWBA calculations for the specified entrance and exit channels [18].

Reaction channel	V_V (MeV)	r_V (fm)	a_V (fm)	V_W (MeV)	r_W (fm)	a_W (fm)	r_C (fm)
^{3}He+^{9}Be	103.9	0.7	0.777	23.81	0.854	0.817	0.767
α+^{8}Be$_{gs}$	121.0	0.252	1.010	17.0 (14.9 [1])	1.38	0.34	0.724
α+^{8}Be$_{3.03}$	121.0	0.252	1.010	17.0 (8.70 [1])	1.38	0.34	0.724

[1] The values obtained in this work.

As can be seen from Figure 2, curves DWBA-1 calculated using the entrance and exit channel potentials with the parameters from [18] differ slightly from the experimental data for the ^{9}Be(^{3}He,α)^{8}Be$_{gs}$ reaction channel, but underestimate the data on the ^{9}Be(^{3}He,α)^{8}Be$_{3.03}$ reaction channel in the angular range of 30–90°. Such a discrepancy between the DWBA calculations and the experimental data can be eliminated either by varying the values of the spectroscopic amplitudes or by reducing the depth V_W of the imaginary part of the exit channel potential [41,42]. We chose the second option, because the values of the spectroscopic amplitudes were obtained in [18] within the framework of the shell model calculations. Therefore, for better description of the experimental data, we reduced the depth V_W of the imaginary part of the exit channel potential (curves DWBA-2), i.e., V_W was obtained by fitting to the neutron transfer data. For the core-core potential (^{3}He+^{8}Be), we used the parameters of the entrance channel potential. The parameters of the optical potential (1) obtained for the entrance and exit channels are presented in Table 1.

The potential parameters for the exit channel α+^{8}Be were obtained through a χ^2 minimization procedure based on the experimental data for the same reaction channel ^{3}He(^{9}Be,α)^{8}Be with fixed spectroscopic amplitudes and potential parameters for the entrance channel, i.e., the elastic scattering channel ^{3}He+^{9}Be. It was found that the parameters of the fitted potential have unusually low values r_V = 0.252 fm and a_W = 0.34 fm; however, they are similar to those found for the α+^{8}Be system in Ref. [43].

The discrepancy between the calculated differential cross sections and the experimental data for the ^{9}Be(^{3}He,α)^{8}Be$_{gs}$ reaction channel around the scattering angle of 55° in Figure 2a may be attributed to the following factors:

(i) The ^{8}Be and ^{9}Be nuclei have a pronounced α-cluster structure which can be incorporated into three-body wave functions for better description of the data [2–4].

 doi:10.20944/preprints202410.2284.v1

(ii) Because of its α-cluster structure, the ^{9}Be nucleus has a large deformation, while in this study it was treated as spherical for simplicity [44].

(iii) It is possible that channel coupling effects are present, as observed in Refs [17,45]. Indeed, the waves with different neutron transfer configurations, originating from multiple channels (e.g., from the ground state and the first excited state), may either cancel each other out or amplify one another; their interference may be taken into account.

Accounting for these factors could lead to an improved theoretical description of the experimental data, but goes beyond the scope of this work.

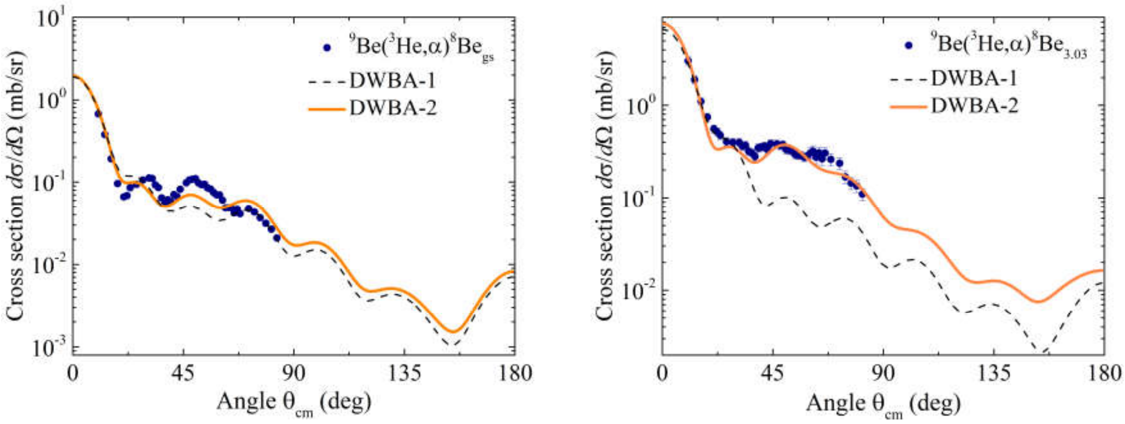

(**a**) (**b**)

Figure 2. Experimental angular distributions (circles) for the reaction channels (**a**) ^{9}Be(^{3}He,α)^{8}Be$_{gs}$ and (**b**) ^{9}Be(^{3}He,α)^{8}Be$_{3.03}$ in comparison with the results of calculations (curves) in the center of mass frame: DWBA-2 (with the potential parameters from [12]) and DWBA-1 (with the reduced depth of the imaginary part of the exit channel potential).

To describe the dynamics of the ^{9}Be(^{3}He,α)^{8}Be$_{gs}$ reaction channel within the TDSE approach, we used the potential obtained for the ^{3}He+^{9}Be entrance channel (Table 1) and the shell model potentials from the DWBA calculations, which yielded curves DWBA-2 in Figure 2.

4. Formalism of the TDSE Approach

The theoretical approach is based on the numerical solution of the time-dependent Schrödinger equation [28–31]

$$i\hbar\frac{\partial}{\partial t}\Psi(\vec{r},t)=-\frac{\hbar^2}{2m}\Delta\Psi(\vec{r},t)+ \\ +\left\{V_1\left(\left|\vec{r}-\vec{r}_1(t)\right|\right)+V_2\left(\left|\vec{r}-\vec{r}_2(t)\right|\right)+V_{LS}^{(1)}\left(\vec{r}-\vec{r}_1(t)\right)+V_{LS}^{(2)}\left(\vec{r}-\vec{r}_2(t)\right)\right\}\Psi(\vec{r},t), \quad (6)$$

where $\Psi(\vec{r},t)$ is the wave function of the neutron with mass m; $\vec{r}_1(t), \vec{r}_2(t)$ are the centers of nuclei moving along classical trajectories; V_1, V_2 are the potentials of interaction of the neutron with the projectile and target nuclei; $V_{LS}^{(1)}$, $V_{LS}^{(2)}$ are the potentials of spin-orbit interaction of the neutron with the cores.

As mentioned above, the neutron wave function at the initial moment of time was determined in the shell model with the parameters obtained in Section 3 and providing the energy of the single-particle level $1p_{3/2}$ equal to the experimental value of the neutron separation energy (1.66 MeV) for the ^{9}Be nucleus [46]. The shape of the ^{9}Be nucleus was considered as spherical [28–30], because taking into account the deformation of ^{9}Be [47] requires more complex calculations, which will be a subject of a separate theoretical work in the future. In addition, it should be noted that taking into account the deformation of weakly bound nuclei in the calculations within the TDSE approach does not have a strong effect on the resulting probabilities and cross sections of transfer reaction channels [28,29]. One of the reasons is that the wave functions calculated in the shell model for deformed and spherical nuclei have similar spatial extents due to the low binding energy of an outer neutron in such nuclei [48].

The wave function $\Psi(\vec{r},t)$ of the neutron with the projection m_j of the total momentum at the initial moment of time can be written as

$$\tilde{\Psi}^{(0)}_{m_j}(\vec{r},t=0)=\begin{bmatrix}\tilde{\psi}^{(0)}_{m_j}(\vec{r},t=0)\\ \tilde{\varphi}^{(0)}_{m_j}(\vec{r},t=0)\end{bmatrix}=\begin{bmatrix}\psi^{(0)}_{m_j}\{\vec{r}-\vec{r}_2(t=0)\}\\ \varphi^{(0)}_{m_j}\{\vec{r}-\vec{r}_2(t=0)\}\end{bmatrix}\exp\left[i\hbar^{-1}m\vec{v}_2(t=0)\vec{r}\right], \tag{7}$$

where $\tilde{\Psi}$ and $\tilde{\varphi}$ are the components of the spinor wave function for the spin projections 1/2 and –1/2, respectively; m is the mass of a neutron; $v_2(t)$ is the velocity of the target nucleus in the center of mass system [28–30]. Evolution of the probability density $\rho(\vec{r},t)$ is calculated as

$$\rho(\vec{r},t)=\frac{1}{(2j+1)}\sum_{-m_j}^{m_j}\left|\psi_{m_j}(\vec{r},t)\right|^2+\left|\varphi_{m_j}(\vec{r},t)\right|^2. \tag{8}$$

For the neutron from the single-particle level $1p_{3/2}$ of the ^{9}Be nucleus, the values of m_j are –3/2, –1/2, 1/2, and 3/2.

The probability of the neutron transfer is determined as

$$P_{\text{tr}}(t)=\sum_k\left|a_k(t)\right|^2, \tag{9}$$

$$a_k(t)=\int\left[\tilde{\psi}^*_k(\vec{r},t)\psi(\vec{r},t)+\tilde{\varphi}^*_k(\vec{r},t)\varphi(\vec{r},t)\right]dV, \tag{10}$$

where $a_k(t)$ are the amplitudes of the probabilities of populating the unoccupied single-particle neutron levels [30]. The final probability of the neutron transfer is determined at time t, when the nuclei are already far away from each other, in our calculations, at distances more than 30 fm:

$$\bar{P}_{\text{tr}}=\lim_{t\to\infty}P_{\text{tr}}(t). \tag{11}$$

The calculated probabilities $\bar{P}_{\text{tr}}$ were approximated by the exponential function

$$\bar{P}_{\text{tr}}(R_{\min})=\min\{\exp(a_0-b_0R_{\min}),1\} \tag{12}$$

with fitting parameters a_0 and b_0 [26].

The probability of the removal of the neutron is determined as

$$P_{\text{rem}}(t)=1-\left|c(t)\right|^2, \tag{13}$$

Preprints.org (www.preprints.org) | NOT PEER-REVIEWED | Posted: 30 October 2024 doi:10.20944/preprints202410.2284.v1

$$c(t) = \frac{1}{(2j+1)} \sum_{-m_j'}^{m_j'} \sum_{-m_j}^{m_j} \int \left[\tilde{\psi}^{(0)*}_{m_j'}(\vec{r},t)\psi_{m_j}(\vec{r},t) + \tilde{\varphi}^{(0)*}_{m_j'}(\vec{r},t)\varphi_{m_j}(\vec{r},t) \right] dV , \tag{14}$$

where $c(t)$ is the amplitude of the probability of conservation of the neutron in the initial state at time t [30]. Similar to the probability of the neutron transfer (11), the final probability of the neutron removal is determined at time t, when the nuclei are already far away from each other:

$$\bar{P}_{\text{rem}} = \lim_{t \to \infty} P_{\text{rem}}(t) . \tag{15}$$

The calculated probabilities $\bar{P}_{\text{rem}}$ were approximated by the sum of two exponential functions:

$$\bar{P}_{\text{rem}}(R_{\min}) = \min\left\{ \exp(a_1 - b_1 R_{\min}) + \exp(a_2 - b_2 R_{\min}), 1 \right\} \tag{16}$$

with fitting parameters a_1, b_1, a_2, b_2 [26].

The numerical solution of equation (4) was performed on a spatial grid of dimensions 96×60×105 fm^3 (x×y×z) with the collision plane xOz and a grid step 0.3 fm [28–30]. We used the dimensionless time scale $\tau = t/t_0$, where $t_0 = m x_0^2/\hbar = 1.57 \cdot 10^{-23}$ s, $x_0 = 1$ fm. The dimensionless time step was $\Delta\tau$ = 0.1. The calculations were carried out using the heterogeneous computing cluster HybriLIT [49] of the Laboratory of Information Technologies, Joint Institute for Nuclear Research.

5. Results and Discussion

Evolution of the probability density (6) in dimensionless time τ for the neutron from the single-particle level $1p_{3/2}$ of the ^{9}Be nucleus during the collision of ^{3}He+^{9}Be at an energy of E_{lab} = 30 MeV ($E_{\text{c.m.}}$ = 22.5 MeV) with the impact parameter b = 6 fm (the distance of the closest approach $R_{\min}$ = 6.12 fm) and b = 8 fm ($R_{\min}$ = 8.23 fm) is presented Figures 3 and 4, respectively. The transition of the neutron probability density begins when the distance between the centers of the nuclei decreases to 9-10 fm [Figures 3a and 4a]. As can be seen from Figures 3b and 4b, the relative velocity of the nuclei is high enough that the flux of the neutron probability density lags behind the motion of the two nuclei and is shifted relative to the imaginary line connecting their centers. A more intense rearrangement of the probability density occurs at small distances between the projectile and target. As the distance between the nuclei increases, the neutron transfer is accompanied by the neutron transition to the continuum [Figures 3c and 4c] [34]. In Figures 3c and 4c, the neutron is emitted at a large angle to the direction of motion of the projectile nucleus, which indicates the manifestation of the so-called *towing mode* at energies above 5 MeV/nucleon [34,50,51].

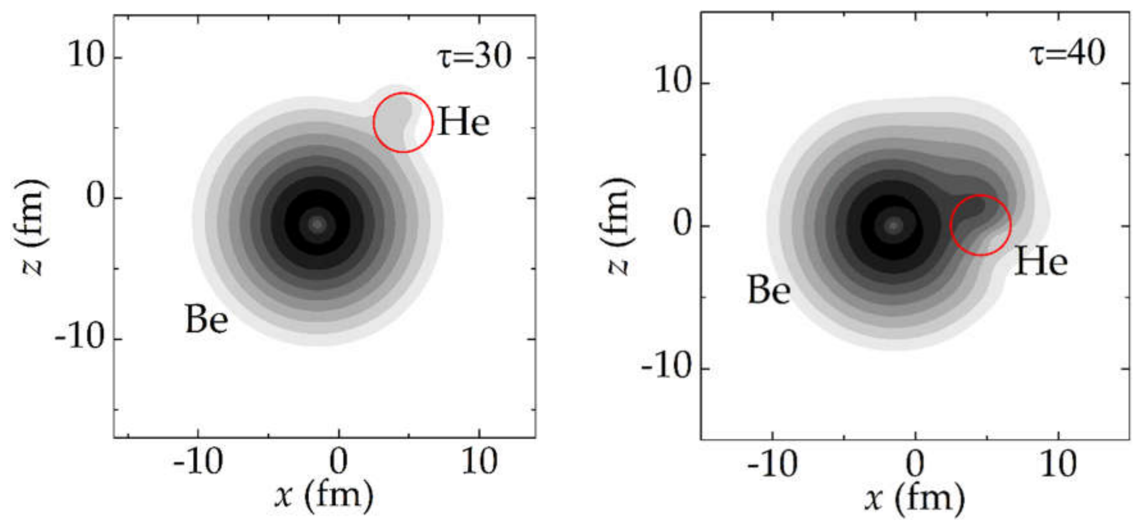

Preprints.org (www.preprints.org) | NOT PEER-REVIEWED | Posted: 30 October 2024 doi:10.20944/preprints202410.2284.v1

(a) (b)

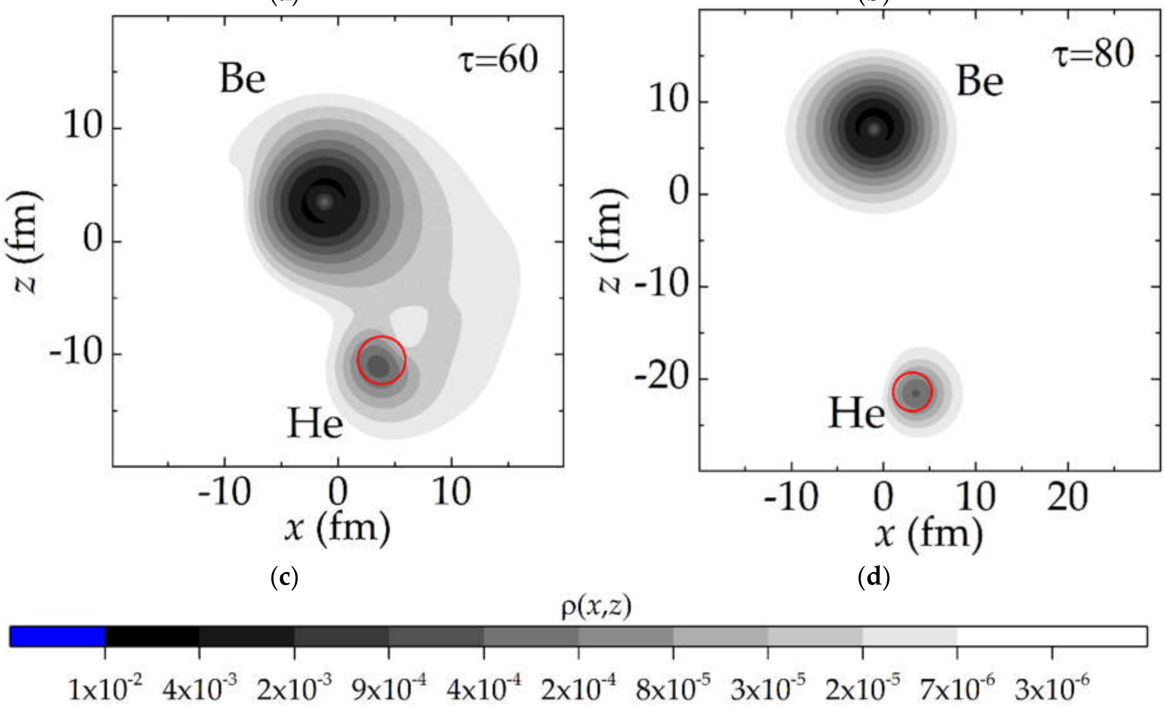

Figure 3. Evolution of the probability density (logarithmic scale; x and z are the coordinates in the collision plane) in dimensionless time τ [(**a**), (**b**), (**c**), (**d**)] for the neutron from the single-particle level $1p_{3/2}$ of the ^{9}Be nucleus during the collision of ^{3}He+^{9}Be at an energy of E_{lab} = 30 MeV ($E_{c.m.}$ = 22.5 MeV) with the impact parameter b = 6 fm (the distance of the closest approach R_{min} = 6.12 fm).

According to the shell model, the ^{3}He nucleus has only one single-particle level $1s_{1/2}$ that can be occupied by the neutron transferred from the single-particle level $1p_{3/2}$ of the ^{9}Be nucleus. The spherically symmetric shape of the part of the neutron probability density transferred to the ^{3}He projectile nucleus in Figures 3d and 4d indicates the population of the state $1s_{1/2}$ in ^{3}He, which is consistent with the shell model.

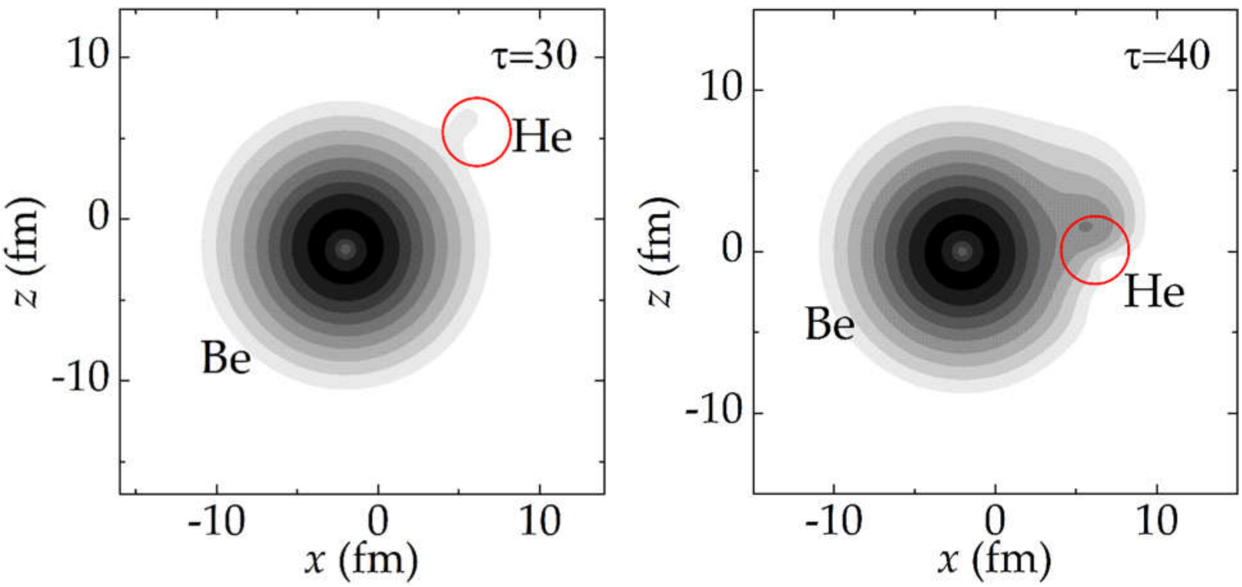

(a) (b)

Preprints.org (www.preprints.org) | NOT PEER-REVIEWED | Posted: 30 October 2024 doi:10.20944/preprints202410.2284.v1

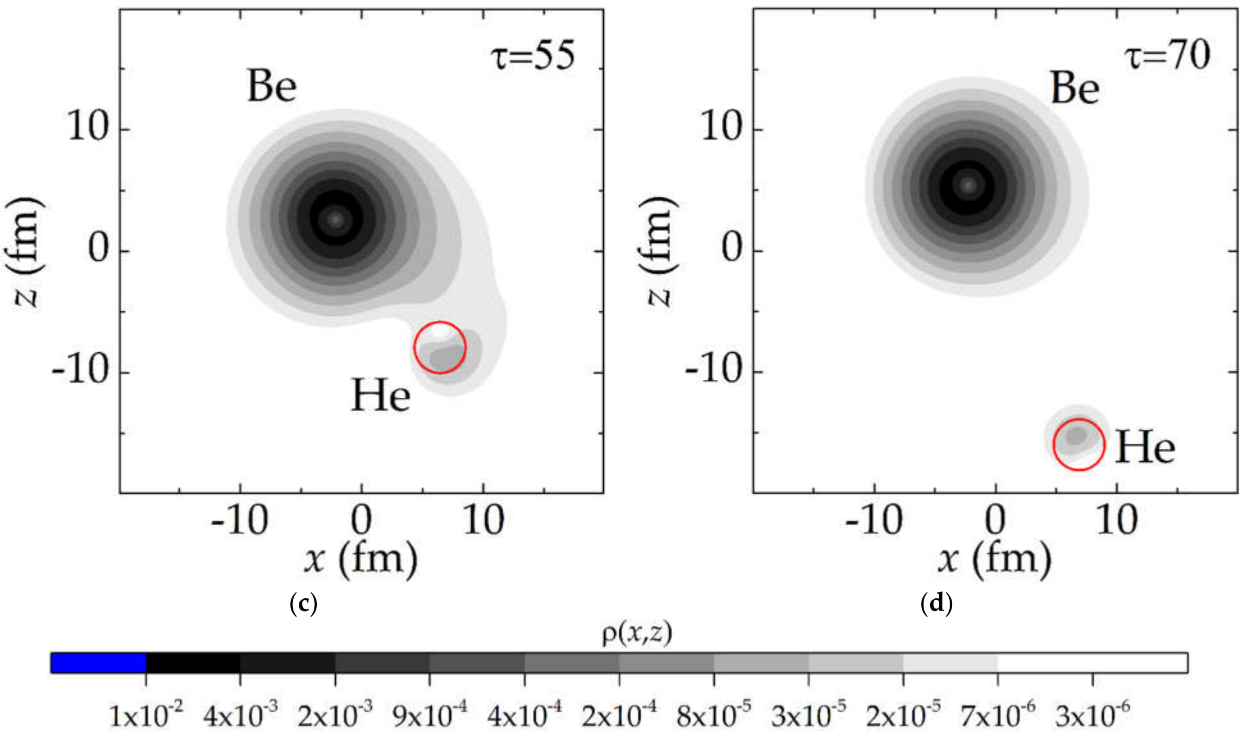

Figure 4. The same as in Figure 3, but for b = 8 fm (R_{min} = 8.23 fm).

The obtained dependencies of the probability $\overline{P}_{tr}$ (11,) (12) on the distance R_{min} of the closest approach of the centers of the nuclei are shown in Figure 5a; the values of the fitting parameters are a_0=0.696 and b_0=0.515 fm^{-1}.

The obtained dependencies of the probability $\overline{P}_{rem}$ (15), (16) on the distance R_{min} of the closest approach of the centers of the nuclei are shown in Figure 5b; the values of the fitting parameters are a_1=1.178, b_1=0.362 fm^{-1}, a_2=–2.08, b_2=0.011 fm^{-1}. The first exponential function describes a rapid decrease of the probability $\overline{P}_{loss}$ at the values of R_{min}, not greatly exceeding the Coulomb barrier radius, the second corresponds to a slow decrease at larger values and gives the main contribution at R_{min} more than 9 fm. The rapid decrease of the probability $\overline{P}_{loss}$ is due to a sharp decrease of the probability of the neutron transfer $\overline{P}_{tr}$ with the increasing impact parameter.

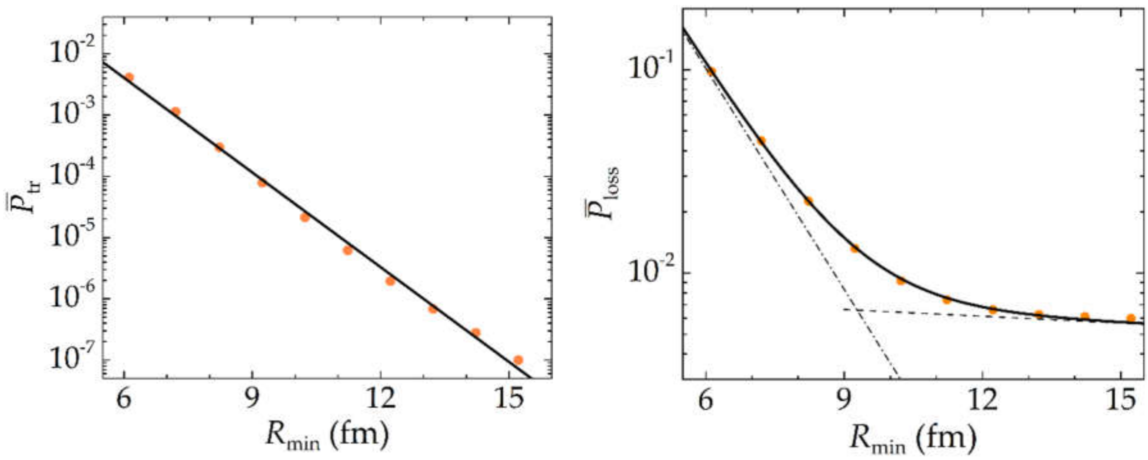

(a) (b)

Figure 5. (**a**) The final neutron transfer probability $\overline{P}_{tr}$: circles are the result of calculations by (11); line is the result of approximation (12). (**b**) The final neutron removal probability $\overline{P}_{rem}$: circles are the

Preprints.org (www.preprints.org) | NOT PEER-REVIEWED | Posted: 30 October 2024 doi:10.20944/preprints202410.2284.v1

result of calculations by (15); solid curve is the result of approximation (16); dashed and dash-dotted lines are the respective contributions of the exponential functions with a_1, b_1, and a_2, b_2 to approximation (16).

In the TDSE approach, the cross sections for the transfer and removal of the weakly bound neutron of the ^{9}Be nucleus were calculated by integrating over the impact parameter b [29,31]

$$\sigma_{tr} = 2\pi \int_{b_{min}}^{\infty} \bar{P}_{tr}\left[R_{min}(b)\right] b db, \quad (17)$$

$$\sigma_{rem} = 2\pi \int_{b_{min}}^{\infty} \bar{P}_{rem}\left[R_{min}(b)\right] b db, \quad (18)$$

where b_{min} is the impact parameter corresponding to the trajectory, when the projectile is still captured by the target. In our calculations, we used b_{min} corresponding to the distance of the closest approach $R_{min} = R_C + d$, where $R_C = 5.6$ fm is the Coulomb barrier radius, $d = 0.4$ fm is the diffuse region, therefore $R_{min} = 6$ fm.

The comparison of the integrated cross sections σ_{tr} for the reaction channel ^{9}Be(^{3}He,α)^{8}Be$_{gs}$ obtained within the DWBA method (FRESCO code) and within the TDSE approach is presented in Table 2. It can be seen that the calculations in both models give close values. Taking into account that the differential cross sections obtained within the DWBA method are slightly below the experimental points in the region of angles around 55°, it can be concluded that the cross sections obtained within the TDSE approach are closer to the experimental data.

The integrated cross section σ_{tr} for the reaction channel ^{9}Be(^{3}He,α)^{8}Be$_{3.03}$ obtained within the DWBA method is also presented in Table 2. The cross section value for this reaction channel is approximately twice as high as that for ^{9}Be(^{3}He,α)^{8}Be$_{gs}$, which is consistent with the measured energy spectrum [Figure 1b], where the number of events for ^{8}Be$_{3.03}$ is approximately twice as high as that for ^{8}Be$_{gs}$.

Table 2 also includes the integrated cross section σ_{rem} for the removal of the weakly bound neutron of the ^{9}Be nucleus obtained within the TDSE approach. According to (13), $\sigma_{rem} = 315.690$ mb includes the neutron transfer cross section $\sigma_{tr} = 0.740$ mb in the reaction channel ^{9}Be(^{3}He,α)^{8}Be$_{gs}$ and the cross section for the transition of the neutron into the continuum. It can be seen that the neutron transfer cross section σ_{tr} makes an insignificant contribution to the neutron removal cross section σ_{rem}.

Table 2. Calculated cross sections.

Reaction channel	**^{9}Be(^{3}He,α)^{8}Be$_{gs}$**	**^{9}Be(^{3}He,α)^{8}Be$_{gs}$**	**^{9}Be(^{3}He,α)^{8}Be$_{3.03}$**	**^{9}Be+^{3}He→^{8}Be$_{gs}$**
Cross section (mb)	σ_{tr} (gs, DWBA) 0.594	σ_{tr} (gs, TDSE) 0.740	σ_{tr} (3.03, DWBA) 1.375	σ_{rem} (TDSE) 315.690

6. Conclusions

The angular distributions for the neutron transfer channels ^{9}Be(^{3}He,α)^{8}Be$_{gs,3.03}$ in the reaction of the ^{3}He (30 MeV) ions with the ^{9}Be target were measured. The experimental data were described by the DWBA method (FRESCO code). The results of the theoretical description are in agreement with the experimental data.

The parameters of the potentials for the ^{3}He+^{9}Be entrance channel and for the shell model obtained from the DWBA calculations were successfully used in the description of dynamics of the reaction channel ^{9}Be(^{3}He,α)^{8}Be$_{gs}$ within the TDSE approach. It has been shown that the neutron transfer process begins when the nuclei approach each other at a distance of 9-10 fm between the centers of the nuclei and the transfer process is accompanied by transition of the neutron to the continuum. In addition, the neutron can be emitted at a large angle to the direction of motion of the projectile nucleus, which indicates the manifestation of the *towing mode*.

The neutron transfer cross section does not make a significant contribution to the cross section for the removal of the weakly bound neutron of the ^{9}Be nucleus. Calculations of the cross section for the reaction channel ^{9}Be(^{3}He,α)^{8}Be$_{gs}$ in the TDSE approach and DWBA method give close values.

Author Contributions: Conceptualization, A.A., E.A., M.N. and K.M.; methodology, T.I.; software, A.A. and E.A.; validation, A.A., S.L. and M.N.; formal analysis, M.N. and K.D.; investigation, A.A., T.I., B.U., K.D., A.K., S.L. and K.M.; resources, K.M. and T.Zh.; data curation, T.I., K.M. and T.Zh.; writing—original draft preparation, K.M.; writing—review and editing, K.O., A.A. and M.N.; visualization, E.A. and B.U.; supervision, A.A.; project administration, K.M.; funding acquisition, T.Zh., K.D. and K.M. All authors have read and agreed to the published version of the manuscript.

Funding: This research was funded by the SCIENCE COMMITTEE OF THE MINISTRY OF SCIENCE AND HIGHER EDUCATION OF THE REPUBLIC OF KAZAKHSTAN, grant number AP14870958.

Data Availability Statement: All data obtained during the study are included in this paper. For any questions regarding the data in the paper, you can contact the corresponding authors.

Acknowledgments: We would like to express our gratitude to the team of the U-120M cyclotron, Nuclear Physics Institute, Řež, Czech Republic for the opportunity to conduct the experiment. We also thank the team of the HybriLIT computing cluster for the opportunity of using its resources.

Conflicts of Interest: The authors declare no conflicts of interest.

References

1. Villanueva G., Moro A.M., Casal J., Lei Jin. Neutron-transfer induced breakup of the Borromean nucleus ^{9}Be. *Phys. Lett. B* **2024**, 855, 138766. DOI 10.1016/j.physletb.2024.138766
2. Fulton B.R., Cowin R.L., Woolliscroft R.J. et al. Exclusive breakup measurements for ^{9}Be. *Phys. Rev. C* **2004**, 70, 047602. DOI 10.1103/PhysRevC.70.047602
3. Prezado Y., Borge M.J.G., Diget C.Aa. et al. Low-lying resonance states in the ^{9}Be continuum. *Phys. Lett. B* **2005**, 618, 43–50. DOI 10.1016/j.physletb.2005.05.030
4. Álvarez-Rodríguez R., Jensen A.S., Garrido E., Fedorov D.V. Structure and three-body decay of ^{9}Be resonances. *Phys. Rev. C* **2010**, 82, 034001. DOI 10.1103/PhysRevC.82.034001
5. Soukeras V., Sgouros O., Pakou A. et al. Global study of ^{9}Be+p at 2.72A MeV. *Phys. Rev. C* **2020**, 102, 064622. DOI 10.1103/PhysRevC.102.064622
6. Von Oertzen W., Freer M., Kanada En'yo Y. Nuclear clusters and nuclear molecules. *Phys. Rep.* **2006**, 432, 43-113. DOI 10.1016/j.physrep.2006.07.001
7. Freer M. The clustered nucleus–cluster structures in stable and unstable nuclei. *Rep. Prog. Phys.* **2007**, 70, 2149. DOI 10.1088/0034-4885/70/12/R03
8. Samarin V.V. Study of spatial structures in α-cluster nuclei. *Eur. Phys. J. A* **2022**, 58, 117. DOI 10.1140/epja/s10050-024-01379-3
9. Bazhin A.S., Samarin V.V. Study of the Structure of the ^{9}Be Nucleus in the Alpha-Cluster Model by the Method of Hyperspherical Functions. *Bulletin of the Russian Academy of Sciences: Physics* **2024**, 88, 1177–1184. DOI 10.1134/S1062873824707281
10. Rakityansky S.A. Wave function of ^{9}Be in the three-body ($\alpha\alpha n$) model. *Phys. Rev. C* **2024**, 110, 024001. DOI 10.1103/PhysRevC.110.024001
11. Tilley D.R., Kelley J.N., Godwin J.L. et al. Energy levels of light nuclei A = 8,9,10. *Nucl. Phys. A* **2004**, 745, 155. DOI 10.1016/j.nuclphysa.2004.09.059
12. Nyman G., Azuma R.E., Hansen P.G. The beta decay of ^{9}Li to levels in ^{9}Be: A new look. *Nucl. Phys. A* **1990**, 510, 189–208. DOI 10.1016/0375-9474(90)90236-F
13. Keeley N., Alamanos N., Rusek K., Kemper K.W. Generation of a repulsive dynamic polarization potential by transfer couplings. *Phys. Rev. C* **2005**, 71, 014611. DOI 10.1103/PhysRevC.71.014611
14. Pandit S.K., Jha V., Mahata K., Santra S. et al. Investigation of cluster structure of ^{9}Be from high precision elastic scattering data. *Phys. Rev. C* **2011**, 84, 031601. DOI 10.1103/PhysRevC.84.031601
15. Saduyev N., Nassurlla M., Burtebayev N. et al. Scattering and One Neutron Pick-Up Reaction on a ^{10}B Target with Deuterons at an Energy of 14.5 MeV. *Physics* **2024**, 6, 1098–1110. DOI 10.3390/physics6030068
16. Lukyanov S.M., Harakeh M.N., Naumenko M.A. et al. Cluster Structure of ^{9}Be from ^{3}He+^{9}Be Reaction. *J. Phys. Conf. Ser.* **2016**, 724, 012031. DOI 10.1088/1742-6596/724/1/012031

17. Urazbekov B.A., Denikin A.S., Lukyanov S.M. et al. Clusterization and strong coupled-channels effects in deuteron interaction with ^{9}Be nuclei. *J. Phys. G Nucl. Part. Phys.* **2019**, 46, 105110. DOI 10.1088/1361-6471/ab37a6
18. Urazbekov B.A., Issatayev T., Lukyanov S.M. et al. Reactions induced by 30 MeV 3He beam on ^{9}Be: cluster transfer reactions. *Chin. Phys. C* **2024**, 48, 014001. DOI 10.1088/1674-1137/ad0376.
19. Azhibekov A.K., Lukyanov S.M., Penionzhkevich Yu.E. et al. Study of one-step and two-step neutron transfer in the reaction ^{6}Li + ^{9}Be. *Chin. Phys. C* **2024**, 48, 114101. DOI 10.1088/1674-1137/ad6d40
20. Urazbekov B.A., Denikin A.S., Sakhiev S.K. et al. Manifestation of the cluster structure of the ^{9}Be nucleus in direct nuclear reactions. *Bull. Russ. Acad. Sci. Phys.* **2016**, 80, 247–251. DOI 10.3103/S1062873816030321
21. Urazbekov B.A., Denikin A.S., Sakhiev S.K. et al. Studying the reactions of deuteron interaction with ^{9}Be nuclei at low energies. *Bull. Russ. Acad. Sci. Phys.* **2017**, 81, 690–694. DOI 10.3103/S1062873817060223
22. Bilwes B., Bilwes R., Ferrero J.L. et al. Mechanism of the ^{9}Be(^{3}He, α)^{8}Be(0) reaction and isoscalar giant resonances of ^{12}C. *J. Phys. France* **1978**, 39, 805–814. DOI 10.1051/jphys:01978003908080500
23. Karban O., Basak A.K., England J.B.A. et al. The j-dependence of (^{3}He, d) and (^{3}He, α) reaction analysing powers in the 1p shell. *Nucl. Phys. A* **1976**, 269, 312–326. DOI 10.1016/0375-9474(76)90683-7
24. Moazed C., Holmgren H.D. Angular correlations for the reaction ^{9}Be(^{3}He, α)^{8}Be (16.92) → α+α. *Phys. Rev.* **1968**, 166, 977. DOI 10.1103/PhysRev.166.977
25. Satchler G. R. Direct Nuclear Reactions; Oxford University Press: New York, USA, **1983**; 833 p.
26. Taylor J.R. Scattering Theory: The Quantum Theory of Nonrelativistic Collisions. Dover Publications: New York, USA, **2006**; 512 p.
27. Thompson I.J. Coupled reaction channels calculations in nuclear physics. *Computer Physics Reports* **1988**, 7, 167–212. DOI 10.1016/0167-7977(88)90005-6; Fresco Coupled Reaction Channels Calculations. Available online: https://www.fresco.org.uk/ (accessed on 10 September 2024).
28. Azhibekov A.K., Samarin V.V., Kuterbekov K.A. Time-dependent calculations for neutron transfer and nuclear breakup processes in ^{11}Li+^{9}Be and ^{11}Li+^{12}C reactions at low energy. *Chin. J. Phys.* **2020**, 65, 292–299. DOI 10.1016/j.cjph.2020.01.009
29. Azhibekov A.K., Samarin V.V. Time-dependent description of reactions with weakly bound ^{11}Li and ^{11}Be nuclei. *Bull. Russ. Acad. Sci.: Phys.* **2022**, 86(9), 1092–1098. DOI 10.3103/S1062873822090064
30. Azhibekov A.K., Lukyanov S.M., Shakhov A.V. et al. Neutron transfer in the ^{48}Ca + ^{197}Au reaction. *Eur. Phys. J. A* **2023**, 59, 278. DOI 10.1140/epja/s10050-023-01192-4
31. Samarin V.V. Time-dependent description of incomplete fusion of nuclei and cluster and nucleon-transfer reactions. *Phys. Atom. Nucl.* **2018**, 81, 486–496. DOI 10.1134/S1063778818040178
32. Valiolda D., Janseitov D., Melezhik V. Investigation of low-lying resonances in breakup of halo nuclei within the time-dependent approach. *Eur. Phys. J. A* **2022**, 58, 34. DOI 10.1140/epja/s10050-022-00684-z
33. Samarin V.V., Naumenko M. A. Study of nucleon-transfer processes in low-energy reactions of helium isotopes with **197**Au Nuclei. *Phys. Atom. Nucl.* **2022**, 85, 880–889. DOI 10.1134/S1063778823010507
34. Lima V., Scarpaci J.A., Lacroix D. et al. Nuclear break-up of ^{11}Be. *Nucl. Phys. A* **2007**, 795, 1-18. DOI 10.1016/j.nuclphysa.2007.07.005
35. Kukulin V.I., Voronchev V.T. Pinch-based thermonuclear D^{3}He fusion driven by a femtosecond laser. *Phys. Atom. Nucl.* **2010**, 73,1376–1383. DOI 10.1134/S1063778810080107
36. Seksembayev Zh., Kukulin V., Sakhiyev S. Study of a dense hot plasma's burning in Z-pinch devices with inertial magnetic confinement. *Phys. Scr.* **2018**, 93, 085602. DOI 10.1088/1402-4896/aacadf
37. Sgouros O., Soukeras V., Pakou A. Low energy proton induced reactions with weakly bound nuclei for application purposes. *Eur. Phys. J. A* **2021**, 57, 125. DOI 10.1140/epja/s10050-021-00447-2
38. Tun Z., Yamani Z., Huang X., Li G., Hartling K., Horn D. Liquid-lithium-cooled beryllium target as the p-to-n converter. *Nucl. Instrum. Methods Phys. Res. A* **2024**, 1064, 169459. DOI 10.1016/j.nima.2024.169459
39. Cyclotron U-120M. Available online: https://www.ujf.cas.cz/en/departments/department-of-accelerators/cyclotron/ (accessed on 10 September 2024).
40. Janseitov D.M., Lukyanov S.M., Mendibayev K. et al. Investigation of the elastic and inelastic scattering of ^{3}He from ^{9}Be in the energy range 30-60 MeV. *Int. J. Mod. Phys. E* **2018**, 27, 1850089. DOI 10.1142/S0218301318500891
41. Micek S., Rebel H., Gils H.J. et al. Single nucleon transfer reactions in ^{6}Li+^{6}Li collisions at 156 MeV. *Z. Phys. A – Atomic Nuclei* **1987**, 328, 467–473. DOI 10.1007/BF01289633
42. Ruby L., Pyle R.V., Wong Yu.-Ch. Cross Sections for ^{6}Li(^{6}Li,^{5}He)^{7}Be, ^{6}Li(d,n)^{7}Be, and ^{19}F(^{6}Li,p)^{24}Na. *Nucl. Sci. Eng.* **1979**, 71, 280-286. DOI 10.13182/NSE79-A19064
43. Cuong D.C. et al. Coupled-reaction-channel study of the ^{12}C(α,^{8}Be) reaction and the ^{8}Be+^{8}Be optical potential. *Phys. Rev. C* **2020**, 102, 024622. DOI 10.1103/PhysRevC.102.024622
44. Sundholm D., Olsen J. Large MCHF calculations on the hyperfine structure of Be(3PO): the nuclear quadrupole moment of ^{9}Be. *Chemical Physics Letters* **1991**, 177, 91-97. DOI 10.1016/0009-2614(91)90181-8
45. Harakeh M.N, Van Popta J., Saha A., Siemssen R.H. Strong coupled-channels effects in the ^{9}Be(α, t)^{10}B reaction. *Nucl. Phys. A* **1980**, 344, 15-40. DOI 10.1016/0375-9474(80)90429-7

 doi:10.20944/preprints202410.2284.v1

46. Wang M., Audi G., Wapstra A.H. et al. The AME 2012 atomic mass evaluation (II), Tables, graphs and references. *Chin. Phys. C* **2012**, 36, 1603. DOI 10.1088/1674-1137/36/12/003
47. Chart of nucleus shape and size parameters. Available online: http://cdfe.sinp.msu.ru/services/radchart/radmain.html (accessed on 10 September 2024).
48. Azhibekov A.K., Samarin V.V., Kuterbekov K.A., Naumenko M.A. Shell model calculations for deformed Li isotopes. *Eurasian j. phys. funct. mater.* **2019**, 3, 307–318. DOI: 10.29317/ejpfm.2019030403
49. Heterogeneous platform «HybriLIT». Available online: http://hlit.jinr.ru/ (accessed on 10 September 2024).
50. Scarpaci J.A., Beaumel D., Blumenfeld Y. et al. A new phenomenon in heavy ion inelastic scattering: the towing mode. *Phys. Lett. B* 1998, **428**, 241–247. DOI 10.1016/S0370-2693(98)00437-7
51. Lacroix D., Scarpaci J.A., Chomaz Ph. Theoretical description of the towing mode through a time-dependent quantum calculation. *Nucl. Phys. A* **1999**, 658, 273–281. DOI 10.1016/S0375-9474(99)00353-X